ORIGINAL ARTICLE

Production forecast of a multistage fractured horizontal well by an analytical method in shale gas reservoir

Yongming Li[1] · Xianyong You[1] · Jinzhou Zhao[1] · Youshi Jiang[1] · Xuan Pu[1]

Abstract

Industry benefits cannot be obtained from shale gas reservoir without stimulations, due to the ultra-low porosity and permeability of shale. A series of integrated technical measures have been developed for developing shale gas economically, such as horizontal wells and multistage hydraulic fracturing. Combining the above works, we can achieve higher productivity by enlarging stimulated reservoir volume (SRV) and linking fracture network in shale gas reservoirs. In this paper, a novel analytical mathematical model for production forecast of multistage horizontal well was developed based on the seepage theory of fractured well in the dual-medium gas reservoirs. In this model, multi-scale migration mechanism and the complicated morphology of hydraulic fractures in fractured shale gas reservoir were considered. It has been closely solved by the method of well test analysis and mathematical physics. To validate the accuracy of the model in this paper, a well from Changning–Weiyuan shale gas reservoir in China is taken as a real-case application. The calculation results of the model and the actual production data of the well are in good accordance. Meanwhile, the impacts of sensitive factors including desorption, Knudsen diffusion, slip flow, stress sensitivity of micro-fractures and high-velocity non-Darcy flow within hydraulic fractures on cumulative production were analyzed. At last, fracture morphology has been optimized through the model.

Keywords Shale gas · Multi-scale flow · Production forecast · Fracture morphology optimization

List of symbols

K_f	Permeability of micro-fracture system, mD
K_m	Permeability of matrix system, mD
K_{HF}	Permeability of hydraulic fracture
K_{fi}	Initial permeability of micro-fracture system, mD
K_{app}	Apparent permeability, mD
K_{HF}	Permeability of the ith hydraulic fracture, mD
P_i	Initial pressure of formation, MPa
P_f	Pressure of micro-fracture system, MPa
P_m	Pressure of matrix system, MPa
P_L	Langmuir pressure, MPa
P_Z	Conversion pressure changing with reservoir pressure, MPa
$\psi_f(x, y, t)$	Pseudo-pressure of point (x, y) in micro-fracture system at t, MPa²/mPa s
ψ_m	Pseudo-pressure of matrix system, MPa²/mPa s
ψ_f	Pseudo-pressure of micro-fracture system, MPa²/mPa s
ψ_i	Initial pseudo-pressure of the formation, MPa²/mPa s
V_L	Langmuir volume, m³/t
V_{std}	Molar volume of gas under standard conditions, m³/t
ϕ_f	Porosity of natural fracture system, dimensionless
ϕ_m	Porosity of matrix system, dimensionless
τ	Tortuosity of porous medium, dimensionless
v_g	Gas seepage velocity in hydraulic fracture, m/s
β	Turbulent velocity coefficient, dimensionless
$\overline{Z}$	Deviation factor of gas under the average temperature and pressure, dimensionless
n	Shape dimension of cutting matrix, dimensionless
M	Molecular weight of gas, dimensionless
B_g	Volume factor of underground gas, dimensionless
ω	Represents the elastic storativity ratio, dimensionless

✉ Jinzhou Zhao
  zhaojz@swpu.edu.cn

1 State Key Laboratory of Oil and Gas Reservoir Geology and Exploitation, Southwest Petroleum University, Chengdu 610500, Sichuan, China

d_f	Stress sensitivity coefficient of micro-fracture, dimensionless
s	Skin factor, dimensionless
C_{ft}	Comprehensive compressibility factor of micro-fracture system, MPa^{-1}
C_{mt}	Comprehensive compressibility factor of matrix system, MPa^{-1}
$\overline{\mu}$	Viscosity of gas under the average temperature and pressure, mPa s
α	Shape factor, m^{-2}
T	Formation temperature, °C
r_w	Radius of wellbore, m
r_e	Radius of reservoir boundary, m
r_n	Average pore radius of shale matrix, nm
h	Thickness of the pay zone, m
w_i	Width of the ith hydraulic fracture, m
x_{frk}	Length of right side of the fracture, m
x_{flk}	Length of left side of the fracture, m
q_a	Desorption amount of shale gas, 10^4 m^3/day
q_{sc}	Gas production of horizontal well under the standard condition, 10^4 m^3/day
q_{ex}	The quality of channeling gas, 10^4 m^3/day
q_i^{HF}	Gas production of the ith hydraulic fracture, 10^4 m^3/day
$q_{l,k,j}^{HF}$	Gas production of the jth segment of left side of the kth hydraulic fracture, 10^4 m^3/day
$q_{r,k,j}^{HF}$	Gas production of the jth segment of right side of the kth hydraulic fracture, 10^4 m^3/day
q_k^{HF}	Gas production of the kth hydraulic fracture, 10^4 m^3/day
$\vec{v}_f$	Darcy velocity of the natural fracture system, m/h
ρ_f	Density of micro-fracture system, kg/m^3
ρ_m	Density of matrix system, kg/m^3
ρ_g	The density of gas, kg/m^3
R	Molar gas constant, $R = 8.314 \times 10^{-3}$ MPa $m^3/$(kmol K)
η_{f+m}	Pressure conductive coefficient of dual-medium gas reservoir, D MPa/(mPa s)
t	Seepage time, h
Y_0	Second type of zero-order Bessel function
Y_1	Second type of first-order Bessel function
J_0	First type of zero-order Bessel function
J_1	First type of first-order Bessel function
$\beta(k)$	Angle between the right side of the fracture's plane with the wellbore, $0 < b < 180°$
$\alpha(k)$	Angle between the left side of the fracture's plane with the wellbore, $0 < a < 90°$

Introduction

Because the permeability and porosity of shale are both ultralow, whose exploration mode and evaluation method are definitely different from conventional gas reservoirs, economic benefits cannot be obtained without multistage fracturing technology. To establish an acknowledged and integrated production forecast model of fractured horizontal wells, enormous researches have been carried out.

Since 1980s, domestic and foreign experts have conducted a lot of theoretical researches on post-fracturing productivity prediction of horizontal wells. Numerical simulation method is widely used, which is more accurate than the analytical method. However, the latter is superior to the former when lacking statistical data.

In terms of numerical simulation, matrix porosity and permeability, fracture length, adsorption and desorption, slippage effect and fracture permeability are considered as principle factors impacting productivity (Frantz et al. 2005; Bustin et al. 2008; Wu et al. 2009). Zhang et al. (2009) innovatively asserted a novel radial composite model to compute the post-fracturing productivity in shale gas reservoirs, which took hydraulic fracture, stimulated reservoir volume (SRV) and fracture network as individual parts (see Fig. 1), similar to our novel model where productivity is calculated through analytical method.

Liu and Yang (2008) derived a formula to calculate the productivity of horizontal wells in low-permeability gas reservoirs on the basis of conformal transformation. Fan et al. (2013) established a model of productivity prediction where
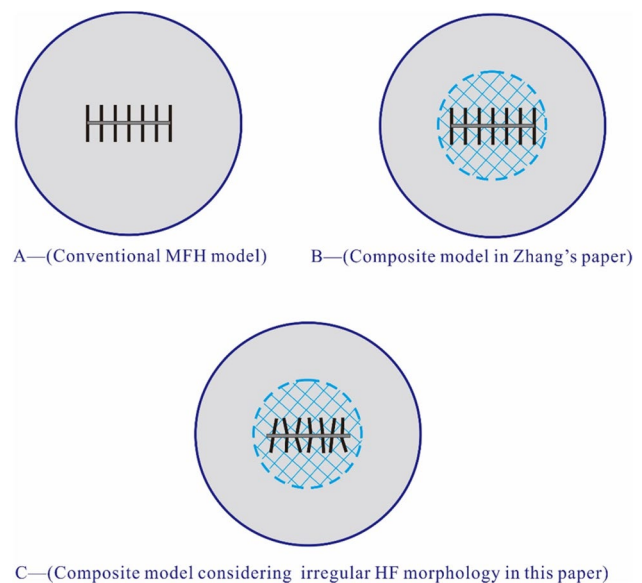

A—(Conventional MFH model)   B—(Composite model in Zhang's paper)

C—(Composite model considering irregular HF morphology in this paper)

Fig. 1 The radial composite model for productivity calculation in shale gas reservoir

slippage effect, stress sensitivity and non-Darcy flow were taken into consideration. Lang et al. (1994) studied the analytical solution of post-fracturing productivity of horizontal wells through potential theory and superposition principle. In addition, some scholars also studied productivity via plate source method and volume source method.

To establish an appropriate model for a better description and prediction of post-fracturing productivity in shale gas reservoirs, the multi-scale seepage mechanism was coupled to Warren and Root model. Kucuk and Sawyer (1980) established a seepage model considering the adsorption and desorption of shale gas and the Klinkenberg effect within nanometer-pore matrix.

As mentioned, multi-scale seepage mechanism means a lot in shale gas reservoirs, so extensive researches have been conducted hitherto. Spivey and Semmelbeck (1995) and Duan et al. (2011) described the adsorption and desorption of shale gas using Langmuir isothermal adsorption equation. Guo et al. (2012) and Swami and Settari (2012) explained the flow process of shale gas in fractures based on Fick's law. Ozkan et al. (2010) asserted that Knudsen flow plays a predominant role when gas flows into fractures from matrix, and established a shale gas seepage model to precisely describe the flow process in the matrix.

In the early period of oilfield exploration, utilizing numerical simulation for production forecast was doubtful owing to its insufficiency of geological data. Hence, analytical formulas got the favor of researchers due to its convenience and quickness (Raghavan and Joshi 1993; Rahman 2008). The core objective of analytical method is to figure out the microcosmic seepage mechanism of shale gas and the representation of fracture network. In this paper, we improved the production forecast method based on the seepage theory in radial composite dual-medium gas reservoir, and a novel model has been established where micro-flow in nanometer-pore matrix, shale gas seepage characteristics in the micro-fracture network, macro-flow feature in the hydraulic fracture and the interference among cracks in the SRV were all taken into account innovatively. This paper is anticipated to present a novel analytical method to predict the post-fracturing production of horizontal wells in shale gas reservoirs.

Physical model and hypothesis

Assuming that SRV in shale gas reservoir is in an elliptic shape, and the length of horizontal well is much less than the radius of reservoir (see Fig. 2), it is considered that SRV locates in the central of the reservoir. Another assumption is that hydraulic fractures have penetrated the play zone, so we define that the intersection of SRV and reservoir is region I, and the rest area is region II. Therefore, region I is
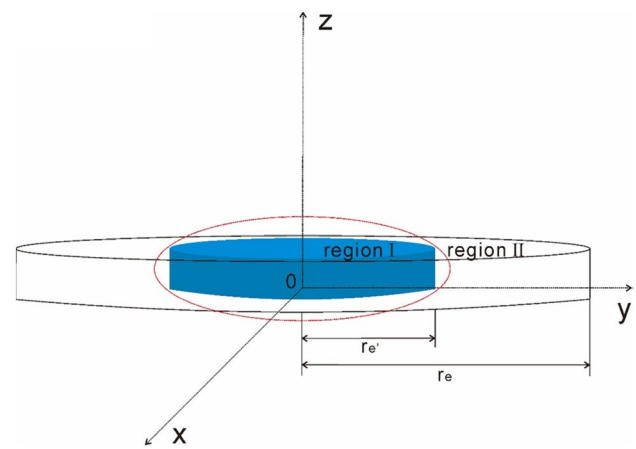

Fig. 2 The radial composite model of fractured horizontal well in shale gas reservoir

an elliptic column whose long axis, minor axis and height are the length of horizontal well, the half-length of hydraulic fracture and the thickness of reservoir, respectively.

Play zones are usually considered as homogeneous medium in prior dual-porosity and dual-permeability models. However, in this paper, fracture network is consisted of macro-hydraulic fractures and micro-induced fractures in SRV based on the corrected Warren and Root model. We assume that post-fracturing reservoir is formed by matrix, natural fracture network out of SRV, micro-fracture network in SRV (which means the zone coupled by rich and well-connected natural fractures and induced fractures), and major hydraulic fractures (Fig. 3). It is more accurate to simplify the realistic reservoir into two radial seepage areas with different porosity and permeability.

To solve the theoretical model analytically, some assumptions should be taken into consideration:

1. The matrix could be dispersed into hexahedron blocks, where micro-fractures and nature fractures inside matrix are interconnected.
2. Isothermal condition is assumed; the gravity and friction effects are ignored.
3. Gas flows into the natural fractures from the source matrix merely and not into the wellbore directly.
4. Shale gas flow in the micro-fracture system is single-phase Darcy flow, while in the nanometer-pore matrix, it is thought as micro-flow such as desorption, diffusion, and slippage.

Correction terms

(1) The radial composite model considering reservoir heterogeneity (Fig. 2).

Fig. 3 The coupled zone sketch composed of radial seepage areas with different porosity and permeability
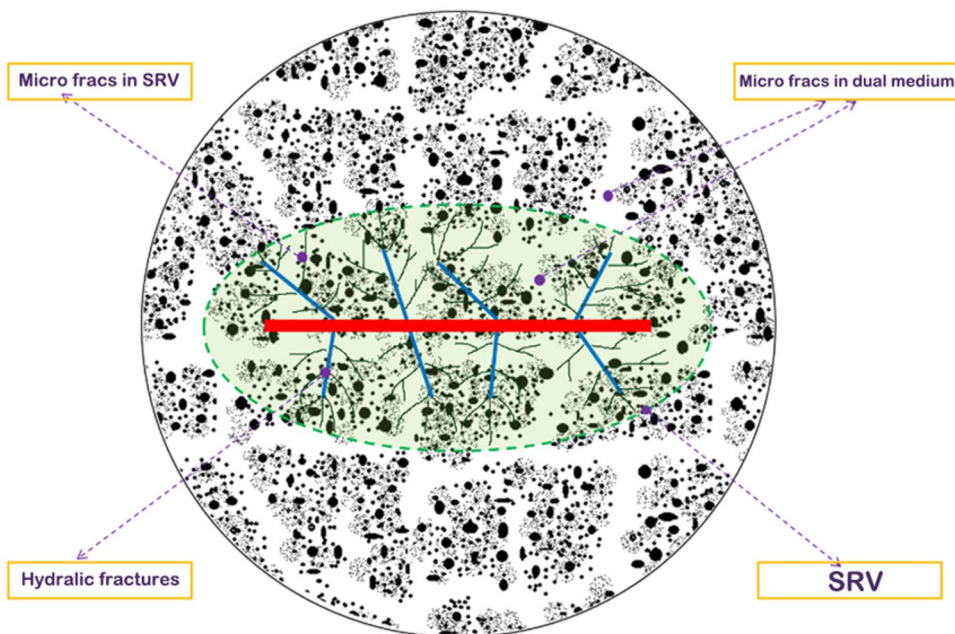
For region I, the porosity and permeability of micro-fracture system is ϕ_m and K_f^I, respectively. That for region II are ϕ_m and K_f^{II}.

(2) Desorption considered in the fluid transport model.

Langmuir model is a primary theoretical model to represent the gas desorption. To express the characteristics of desorption of shale gas, desorption amount can be proposed as follows based on Langmuir isothermal equation (Civan et al. 2011):

$$q_a = \frac{\rho_m M}{V_{std}} \frac{V_L p_m}{p_L + p_m},$$

(1)

where q_a is desorption amount of shale gas, p_L is Langmuir pressure, V_L is Langmuir volume and V_{std} is molar volume of gas under standard conditions.

(3) Micro-flow model considering multi-scale seepage mechanism.

Javadpour (2009) compared theory with experimental results and indicated that flow in nanometer pore can be expressed by Knudsen diffusion where viscous effect is ignored. To characterize the micro-flow of shale gas with Knudsen diffusion and slippage in nanometer pore, apparent permeability model has been introduced:

where K_{app} is apparent permeability, τ is tortuosity of porous medium, r_n is average pore radius of shale matrix nad α is accommodation coefficient of tangential momentum (it is 0.8 in this paper).

(4) Stress sensitivity in micro-fracture system.

The influence of pore pressure on the permeability of micro-fracture could be expressed as the following equation:

$$K_f = K_{fi} \exp\left[-d_f\left(p_{fi} - p_f\right)\right],$$

(3)

where K_f is the permeability of micro-fracture system; K_{fi} is the initial permeability of micro-fracture system; d_f is stress sensitivity coefficient of micro-fracture.

(5) Non-Darcy seepage mathematical model for micro-fractures

Considering the high-speed non-Darcy effect in seepage mathematical model for micro-fractures, non-Darcy coefficient is expressed as

$$\sigma_g = \left(1 + \frac{K_{HF}\beta\rho_g v_g}{\mu_g}\right)^{-1},$$

(4)

$$K_{app} = \frac{\phi_m}{\tau}\left\{\frac{2r_n\mu_g}{3RT\rho_g}\left(\frac{8RT}{\pi M}\right)^{0.5} + \frac{r_n^2}{8}\left[1 + \frac{\mu_g}{p_m r_n}\left(\frac{2}{\alpha} - 1\right)\left(\frac{8\pi RT}{M}\right)^{0.5}\right]\right\},$$

(2)

where K_{HF} is permeability of hydraulic fracture, v_g is gas seepage velocity in hydraulic fracture and β is turbulent velocity coefficient.

Mathematical model

The model of matrix system and micro-fracture network

The derivation process of novel model of horizontal well in fractured shale gas reservoir is similar to that of traditional dual-medium reservoir model, shown in Appendix 1.

Because shale gas cannot be thought as ideal gas, it is inappropriate to use square pressure for establishing the model. To linearize the percolation differential equation, pseudo-pressure is introduced into the model. Then accuracy of the solution can be improved. The percolation differential equation of fractured shale gas reservoir is presented as follows:

$$\begin{cases} \dfrac{3.6K_f}{\bar{\mu}}\left[\dfrac{1}{r}\dfrac{\partial}{\partial r}\left(r\dfrac{\partial \psi_f}{\partial r}\right)\right] + \dfrac{3.6\alpha K_{app}}{\bar{\mu}}(\psi_m - \psi_f) = \phi_f C_{ft}\dfrac{\partial \psi_f}{\partial t} \\ -\dfrac{3.6\alpha K_{app}}{\bar{\mu}}(\psi_m - \psi_f) = \phi_m C_{mt}\dfrac{\partial \psi_m}{\partial t} \\ \psi_m(r,0) = \psi_f(r,0) = \psi_i \\ r\dfrac{\partial \psi_f}{\partial r}\bigg|_{r=r_w} = \dfrac{1.274 \times 10^{-2}\,q_{sc}T}{K_f h} \\ \dfrac{\partial \psi_m}{\partial r}(r_e,t) = \dfrac{\partial \psi_f}{\partial r}(r_e,t) = 0. \end{cases}$$

(5)

The method of variables separation is applied to solve the model (Wu 2008), then pseudo-pressure is separated as

$$\begin{cases} \psi_m(r,t) = f_1(r) - \theta t + u_1(r,t) \\ \psi_f(r,t) = f_2(r) - \theta t + u_2(r,t) \end{cases},$$

(6)

where $f_1(r), f_2(r), u_1(r,t), u_2(r,t)$ can be obtained by solving the equations below:

$$\begin{cases} \dfrac{1}{r}\dfrac{\partial}{\partial r}\left(r\dfrac{\partial f_2}{\partial r}\right) + \dfrac{\alpha K_{app}}{K_f}(f_1 - f_2) = -\dfrac{\bar{\mu}\phi_f C_{ft}}{3.6K_f}\theta \\ 3.6\alpha K_{app}(f_1 - f_2) = \bar{\mu}\phi_m C_{mt}\theta \\ \dfrac{\partial f_2}{\partial r}\bigg|_{r=r_e} = 0 \\ \dfrac{\partial f_2}{\partial r}\bigg|_{r=r_w} = -\dfrac{1.274 \times 10^{-2}\,q_{sc}T}{K_f h r_w} \end{cases},$$

(7)

$$\begin{cases} \dfrac{1}{r}\dfrac{\partial}{\partial r}\left(r\dfrac{\partial u_2}{\partial r}\right) + \dfrac{\alpha K_{app}}{K_f}(u_1 - u_2) = \dfrac{\bar{\mu}\phi_f C_{ft}}{3.6K_f}\dfrac{\partial u_2}{\partial t} \\ -3.6\alpha K_{app}(f_1 - f_2) = \bar{\mu}\phi_m C_{mt}\dfrac{\partial u_1}{\partial t} \\ \dfrac{\partial u_2}{\partial r}\bigg|_{r=r_e} = 0 \\ \dfrac{\partial u_2}{\partial r}\bigg|_{r=r_w} = 0 \\ u_1|_{t=0} = \psi_i - f_1 \\ u_2|_{t=0} = \psi_i - f_2 \end{cases}.$$

(8)

After calculation, the result (see Appendix 2) can be obtained as

$$\psi_f = \psi_i - \dfrac{1.274 \times 10^{-2}q_{sc}T}{K_f h(r_e^2 - r_w^2)}\left[\dfrac{r^2}{2} + r_e^2\left(\ln r_e - \dfrac{1}{2}\right) - r_e^2\ln r - r_w^2\left(\ln r_w - \dfrac{1}{2}\right) - \dfrac{1}{4r_e^2}(r_e^4 - r_w^4)\right]$$
$$- \dfrac{9.173 \times 10^{-2}q_{sc}Tt}{\bar{\mu}h(\phi_m C_{mt} + \phi_f C_{ft})(r_e^2 - r_w^2)} - \dfrac{9.173 \times 10^{-2}q_{sc}T\eta[1 - e^{-(\xi+\eta)t}]}{\bar{\mu}h(\phi_m C_{mt} + \phi_f C_{ft})(r_e^2 - r_w^2)\xi(\xi+\eta)} + \dfrac{q_{sc}T}{2\bar{\mu}h\phi_f C_{ft}r_w\sqrt{X_2}\xi}$$
$$\times \sum_{j=1}^{\infty}\dfrac{J_1^2\left(\sqrt{\frac{\lambda_j}{X_2}}r_e\right)\left[\nu_{+j}(\xi - \nu_{-j})e^{-\nu_{-j}t} - \nu_{-j}(\xi - \nu_{+j})e^{-\nu_{+j}t}\right]}{\sqrt{\lambda_j}(\nu_{+j} - \nu_{-j})\left[J_1^2\left(\sqrt{\frac{\lambda_j}{X_2}}r_w\right) - J_1^2\left(\sqrt{\frac{\lambda_j}{X_2}}r_e\right)\right]}\Phi_{1,0}(r, r_w, \lambda_j),$$

(9)

where $\xi = \dfrac{3.6\alpha K_{app}}{\bar{\mu}\phi_m C_{mt}}, \eta = \dfrac{3.6\alpha K_{app}}{\bar{\mu}\phi_f C_{ft}}, \lambda = \nu\left(\dfrac{\eta}{\xi - \nu} + 1\right), X_2 = \dfrac{3.6K_f}{\bar{\mu}\phi_f C_{ft}},$

$$\begin{cases} \nu_{-j} = \dfrac{1}{2}\left[\xi + \eta + \lambda_j + \sqrt{(\xi + \eta + \lambda_j)^2 - 4\xi + \eta + \lambda_j}\right], & j = 1,2,3,\dots \\ \nu_{+j} = \dfrac{1}{2}\left[\xi + \eta + \lambda_j - \sqrt{(\xi + \eta + \lambda_j)^2 - 4\xi + \eta + \lambda_j}\right], & j = 1,2,3,\dots. \end{cases}$$

(10)

As the expression of pseudo-pressure has been obtained, some simplifications should be conducted to make the solution process more convenient. On the one hand, according to the conclusion of Chen (1983), all terms in the formula can be ignored except the first one. On the other hand, considering that r_w is far less than r_e, r_w/r_e can be thought as 0. So we can obtain the simplification of Eq. (9) as follows:

$$\psi_i - \psi_f(r, t) = \frac{1.274 \times 10^{-2} q_{sc} T}{K_f h} \left\{ \ln \frac{r_e}{r} - \frac{3}{4} + \frac{2\eta_{f+m} t}{r_e^2} + \frac{r^2}{2r_e^2} + \frac{2K_f(1-\omega)^2}{\alpha K_{app} r_e^2} \left[1 - \exp\left(-\frac{\alpha K_{app} \eta_{f+m} t}{K_f \omega(1-\omega)} \right) \right] \right\}. \tag{11}$$

Converting Eq. (11) into the form of plane rectangular coordinates and considering the impact of volume factor B_g, we can deduce it in following form:

$$\psi_i - \psi_f(x, y, t) = \frac{1.274 \times 10^{-2} B_g q_{sc} T}{K_f h}$$

$$\left\{ \ln \frac{r_e}{\sqrt{(x-x_0)^2 + (y-y_0)^2}} - \frac{3}{4} + \frac{2\eta_{f+m} t}{r_e^2} \right.$$

$$\left. + \frac{(x-x_0)^2 + (y-y_0)^2}{2r_e^2} + \frac{2K_f(1-\omega)^2}{\alpha K_{app} r_e^2} \left[1 - \exp\left(-\frac{\alpha K_{app} \eta_{f+m} t}{K_f \omega(1-\omega)} \right) \right] \right\}. \tag{12}$$

Equation (13) could be used for expressing Eq. (12) for simplification:

$$\psi_i - \psi_f(x, y, t) = \psi(x, x_0, y, y_0, q_{sc}). \tag{13}$$

The model of macro-hydraulic fractures

In this paper, angles between hydraulic fracture and wellbore are irregular. Every half fracture should be divided into n segments, and each segment denotes a point (Xu et al. 2006). Set horizontal wellbore as y-axis (see Fig. 4), the coordinate of initial fracture point of kth fracture as $(0, y_{fk})$,

left/right side length of fracture as x_{flk}/x_{frk}, the angle between the left/right side of hydraulic fracture and wellbore as $\alpha(k)(0 < \alpha < 90°)/\beta(k)(0 < \beta < 180°)$. Then the coordinates

Fig. 4 Physical model of a multistage fractured horizontal well in shale gas reservoir
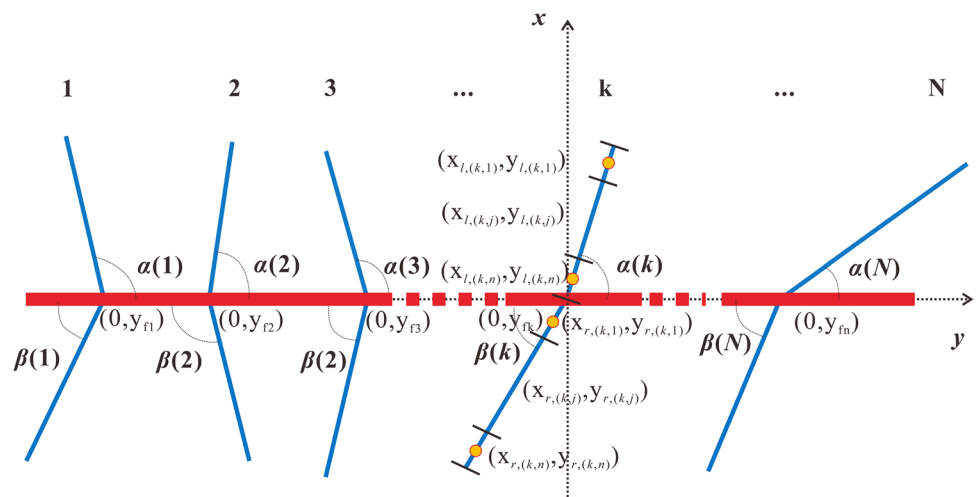
of these points can be expressed by the midpoint coordinates of each segment (Zhao et al. 2016).

In micro-fracture system, the total pseudo-pressure drop of a random point (x, y) impacted by all fractures simultaneously at time t, which can be presented as follows by substituting the points' coordinates into Eq. (12):

Mathematical model solution

The gas flow process from main fractures to horizontal wellbore can be assumed as plane radial flow (Mukherjee and Economides 1991):

$$\psi_i - \psi_i^{HF}(x, y, t) = \frac{1}{2}\sum_{k=1}^{N}\sum_{j=1}^{n}\psi_{late}\left(-\left(1-\frac{1}{2n}\right)x_{l,i}^{HF}\sin\alpha(i), -\frac{1}{2}\left(\frac{2n-2j+1}{n}\right)x_{l,k}^{HF}\sin\alpha(k), y_i^{HF} + \left(1-\frac{1}{2n}\right)x_{l,i}^{HF}\cos\alpha(i), y_k^{HF} + \frac{1}{2}\left(\frac{2n-2j+1}{n}\right)x_{l,k}^{HF}\cos\alpha(k), q_{l,k,j}^{HF}\right)$$

$$+ \frac{1}{2}\sum_{k=1}^{N}\sum_{j=1}^{n}\psi_{late}\left(-\left(1-\frac{1}{2n}\right)x_{l,i}^{HF}\sin\alpha(i), \frac{1}{2}\left(\frac{2j-1}{n}\right)x_{r,k}^{HF}\sin\beta(k), y_i^{HF} + \left(1-\frac{1}{2n}\right)x_{l,i}^{HF}\cos\alpha(i), y_k^{HF} - \frac{1}{2}\left(\frac{2j-1}{n}\right)x_{r,k}^{HF}\cos\beta(k), q_{r,k,j}^{HF}\right)$$

$$+ \frac{1}{2}\sum_{k=1}^{N}\sum_{j=1}^{n}\psi_{late}\left(\left(1-\frac{1}{2n}\right)x_{r,i}^{HF}\sin\beta(i), -\frac{1}{2}\left(\frac{2n-2j+1}{n}\right)x_{l,k}^{HF}\sin\alpha(k), y_i^{HF} - \left(1-\frac{1}{2n}\right)x_{r,i}^{HF}\cos\beta(i), y_k^{HF} + \frac{1}{2}\left(\frac{2n-2j+1}{n}\right)x_{l,k}^{HF}\cos\alpha(k), q_{l,k,j}^{HF}\right)$$

$$+ \frac{1}{2}\sum_{k=1}^{N}\sum_{j=1}^{n}\psi_{late}\left(\left(1-\frac{1}{2n}\right)x_{r,i}^{HF}\sin\beta(i), \frac{1}{2}\left(\frac{2j-1}{n}\right)x_{r,k}^{HF}\sin\beta(k), y_i^{HF} - \left(1-\frac{1}{2n}\right)x_{r,i}^{HF}\cos\beta(i), y_k^{HF} - \frac{1}{2}\left(\frac{2j-1}{n}\right)x_{r,k}^{HF}\cos\beta(k), q_{r,k,j}^{HF}\right),$$

$$(14)$$

$$q_{l,k,j}^{HF} = \frac{x_{l,k}^{HF}}{n\left(x_{l,k}^{HF} + x_{r,k}^{HF}\right)}q_k^{HF}, \tag{15}$$

$$q_{r,k,j}^{HF} = \frac{x_{r,k}^{HF}}{n\left(x_{l,k}^{HF} + x_{r,k}^{HF}\right)}q_k^{HF}, \tag{16}$$

where $q_{l,k,j}^{HF}$ and $q_{r,k,j}^{HF}$ denote the gas production of the jth point of left/right wing of the kth main fracture.

Because gas flows into hydraulic fracture tip from micro-fracture network, we can substitute the tip point coordinates into Eq. (14) and obtain the total formation pseudo-pressure drop when gas flows from matrix into hydraulic fractures.

$$\psi_i^{HF}(x, y, t) - \psi_{wf,i} = \frac{1.291 \times 10^{-3}B_g q_i^{HF}T}{K_{l,i}^{HF}w_i}\left(\ln\frac{\sqrt{\frac{\left(x_{l,i}^{HF}+x_{r,i}^{HF}\right)h}{\pi}}}{r_w} + s\right). \tag{17}$$

Combining the equations presented above, the analytical model for production forecast of multistage fractured horizontal well in shale gas reservoir can be obtained as follows:

Table 1 The parameters of shale gas reservoir

Thickness of reservoir (m)	32	Viscosity of gas (mPa s)	0.026
Initial formation pressure (MPa)	33.49	Bottomhole flow pressure (MPa)	15.87
Permeability of matrix (mD)	2.5×10^{-5}	Porosity of matrix	0.0547
Density of rock (kg/m^3)	2600	Porosity of fracture network	0.005
Permeability of fracture network (region I) (mD)	0.1	Permeability of fracture network (region II) (mD)	3.6×10^{-5}
Boundary radius (m)	1500	Length of horizontal wellbore (m)	1600
Skin factor	0	Proportion of gas	0.7
Formation temperature (°C)	82.2	Coefficient of stress sensitivity (MPa^{-1})	0.05
Tortuosity of porous medium	5	Average pore radius of rock (nm)	5
Accommodation coefficient of tangential momentum	0.8	Practical gas content (m^3/t)	1.71
Langmuir pressure (MPa)	5	Langmuir volume (m^3/t)	2

$$
\begin{aligned}
\psi_i - \psi_{wf,i} = \frac{1}{2} \Bigg\{ & \sum_{k=1}^{N} \Bigg[\sum_{j=1}^{N} \frac{1.274 \times 10^{-2} B_g x_{l,k}^{HF} q_k^{HF} T}{n\left(x_{l,k}^{HF} + x_{r,k}^{HF}\right)\sigma_g K_f h} \left\{ \frac{2\eta_{f+m}t}{r_e^2} - \frac{3}{4} + \frac{2K_f(1-\omega)^2}{\alpha K_{app} r_e^2} \left[1 - \exp\left(-\frac{\alpha K_{app}\eta_{f+m}t}{K_f\omega(1-\omega)}\right) \right] + \ln \frac{r_e}{\sqrt{A}} + \frac{A}{2\,r_e^2} \right\} \\
& + \sum_{j=1}^{N} \frac{1.274 \times 10^{-2} B_g x_{l,k}^{HF} q_k^{HF} T}{n\left(x_{l,k}^{HF} + x_{r,k}^{HF}\right)\sigma_g K_f h} \left\{ \frac{2\eta_{f+m}t}{r_e^2} - \frac{3}{4} + \frac{2K_f(1-\omega)^2}{\alpha K_{app} r_e^2} \left[1 - \exp\left(-\frac{\alpha K_{app}\eta_{f+m}t}{K_f\omega(1-\omega)}\right) \right] + \ln \frac{r_e}{\sqrt{B}} + \frac{B}{2\,r_e^2} \right\} \Bigg] \\
& + \sum_{k=1}^{N} \Bigg[\sum_{j=1}^{N} \frac{1.274 \times 10^{-2} B_g x_{l,k}^{HF} q_k^{HF} T}{n\left(x_{l,k}^{HF} + x_{r,k}^{HF}\right)\sigma_g K_f h} \left\{ \frac{2\eta_{f+m}t}{r_e^2} - \frac{3}{4} + \frac{2K_f(1-\omega)^2}{\alpha K_{app} r_e^2} \left[1 - \exp\left(-\frac{\alpha K_{app}\eta_{f+m}t}{K_f\omega(1-\omega)}\right) \right] + \ln \frac{r_e}{\sqrt{C}} + \frac{C}{2\,r_e^2} \right\} \\
& + \sum_{j=1}^{N} \frac{1.274 \times 10^{-2} B_g x_{l,k}^{HF} q_k^{HF} T}{n\left(x_{l,k}^{HF} + x_{r,k}^{HF}\right)\sigma_g K_f h} \left\{ \frac{2\eta_{f+m}t}{r_e^2} - \frac{3}{4} + \frac{2K_f(1-\omega)^2}{\alpha K_{app} r_e^2} \left[1 - \exp\left(-\frac{\alpha K_{app}\eta_{f+m}t}{K_f\omega(1-\omega)}\right) \right] + \ln \frac{r_e}{\sqrt{D}} + \frac{D}{2\,r_e^2} \right\} \Bigg] \Bigg\} \\
& + \frac{1.291 \times 10^{-3} B_g q_k^{HF} T}{K_i w_i} \left(\ln \frac{\sqrt{\left(x_{l,i}^{HF} + x_{r,i}^{HF}\right)h}}{\sqrt{\pi}\, r_w} + s \right),
\end{aligned}
\tag{18}
$$

where

$$
\begin{aligned}
A = & \left[-\left(1 - \frac{1}{2n}\right)x_{l,i}^{HF}\sin\alpha(i) + \frac{1}{2}\left(\frac{2n-2j+1}{n}\right)x_{l,k}^{HF}\sin\alpha(k) \right]^2 \\
& + \left[y_i^{HF} + \left(1 - \frac{1}{2n}\right)x_{l,i}^{HF}\cos\alpha(i) - y_k^{HF} - \frac{1}{2}\left(\frac{2n-2j+1}{n}\right)x_{l,k}^{HF}\cos\alpha(k) \right]^2,
\end{aligned}
$$

$$
\begin{aligned}
B = & \left[-\left(1 - \frac{1}{2n}\right)x_{l,i}^{HF}\sin\alpha(i) - \frac{1}{2}\left(\frac{2j-1}{n}\right)x_{r,k}^{HF}\sin\beta(k) \right]^2 \\
& + \left[y_i^{HF} + \left(1 - \frac{1}{2n}\right)x_{l,i}^{HF}\cos\alpha(i) - y_k^{HF} + \frac{1}{2}\left(\frac{2j-1}{n}\right)x_{r,k}^{HF}\cos\beta(k) \right],
\end{aligned}
$$

Table 2 The parameters of hydraulic fractures

Frac number	Frac left length (m)	Frac right length (m)	Frac width (mm)	Frac interval (m)	Intersection angle of frac left side (°)	Intersection angle of frac right side (°)	Frac permeability (D)
1	136	126	2.5	110	80	110	2.1
2	123.3	133.3	2.4	110	90	80	2.2
3	121.7	131.7	2.4	100	85	105	1.8
4	137.9	127.9	2.5	120	70	80	2.3
5	119	125	2.5	120	110	115	1.9
6	138	121.6	2.4	130	90	90	1.7
7	114.3	124.3	2.6	110	85	96	2.2
8	126	136	2.5	110	110	80	2.1
9	133.3	123.3	2.4	110	80	90	2.2
10	131.7	121.7	2.4	100	105	85	1.8
11	127.9	137.9	2.5	120	80	70	2.3
12	125	119	2.5	120	115	110	1.9
13	121.6	138	2.4	130	90	90	1.7
14	124.3	114.3	2.6	–	75	75	2.2

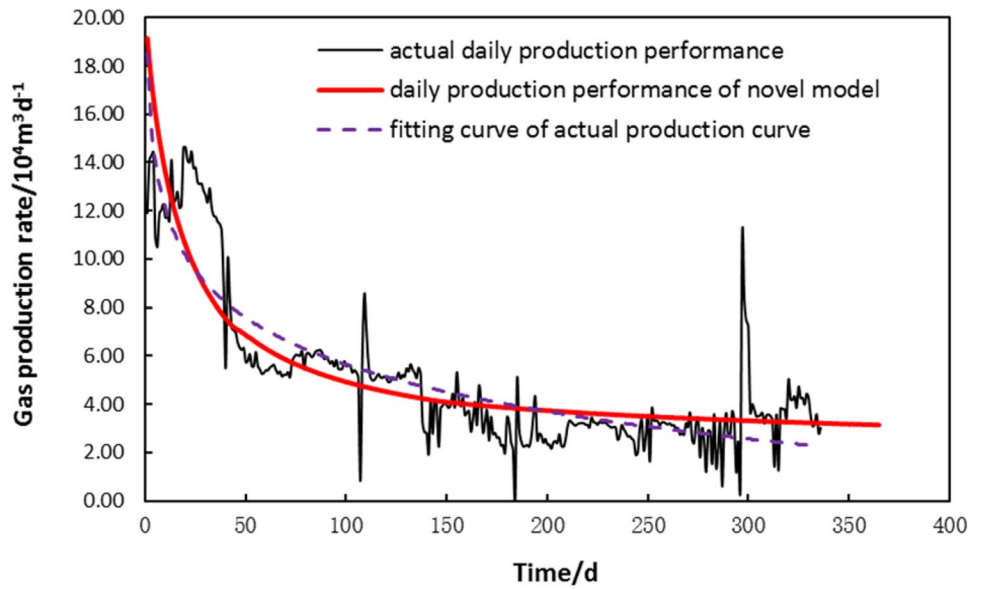**Fig. 5** The simulation production curve and actual production curve of well WH-1

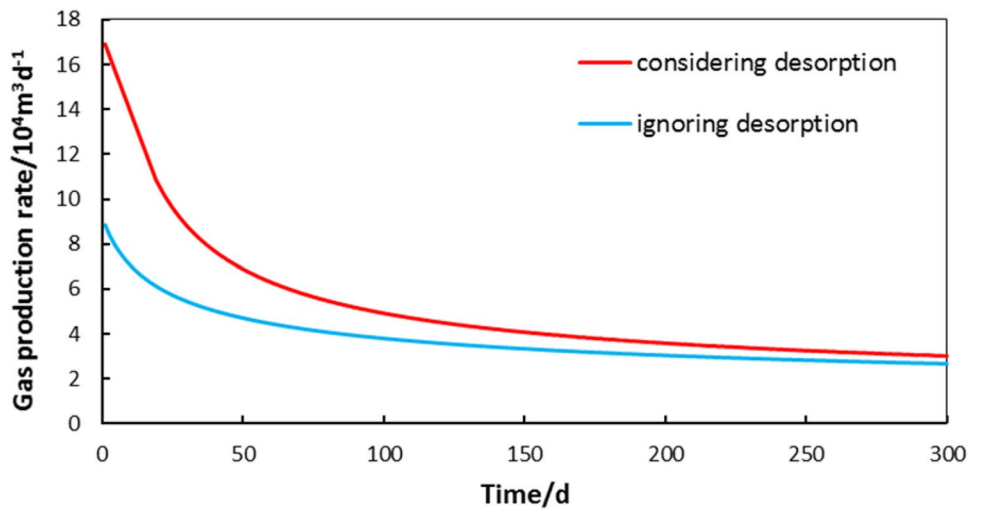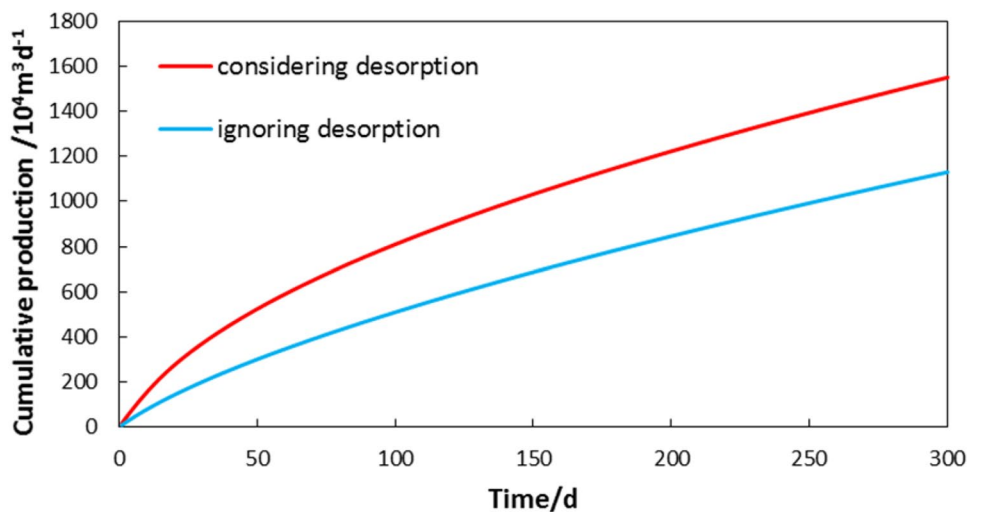**Fig. 6** Influence of desorption on daily production of well WH-1

Fig. 7 Influence of desorption on cumulative production of well WH-1

$$C = \left[\left(1 - \frac{1}{2n}\right) x_{r,i}^{\text{HF}} \sin \beta(i) + \frac{1}{2} \left(\frac{2n - 2j + 1}{n}\right) x_{l,k}^{\text{HF}} \sin \alpha(k) \right]^2$$
$$+ \left[y_i^{\text{HF}} - \left(1 - \frac{1}{2n}\right) x_{r,i}^{\text{HF}} \cos \beta(i) - y_k^{\text{HF}} - \frac{1}{2} \left(\frac{2n - 2j + 1}{n}\right) x_{l,k}^{\text{HF}} \cos \alpha(k) \right],$$

$$D = \left[\left(1 - \frac{1}{2n}\right) x_{r,i}^{\text{HF}} \sin \beta(i) - \frac{1}{2} \left(\frac{2j - 1}{n}\right) x_{r,k}^{\text{HF}} \sin \beta(k) \right]^2$$
$$+ \left[y_i^{\text{HF}} - \left(1 - \frac{1}{2n}\right) x_{r,i}^{\text{HF}} \cos \beta(i) - y_k^{\text{HF}} + \frac{1}{2} \left(\frac{2j - 1}{n}\right) x_{r,k}^{\text{HF}} \cos \beta(k) \right]^2 .$$

Equation (18) is the mathematical model for production forecast in fractured shale gas reservoir. First, sum the whole segments of N fractures; then LU decomposition method can be used to calculate the production of every hydraulic fracture; finally, obtain the total production by summing the production of each fracture.

In this part, the pseudo-pressure of imperfect gas cannot be solved by analytical method easily and some correction

Fig. 8 Influence of Knudsen diffusion and slippage effect on daily production of well WH-1
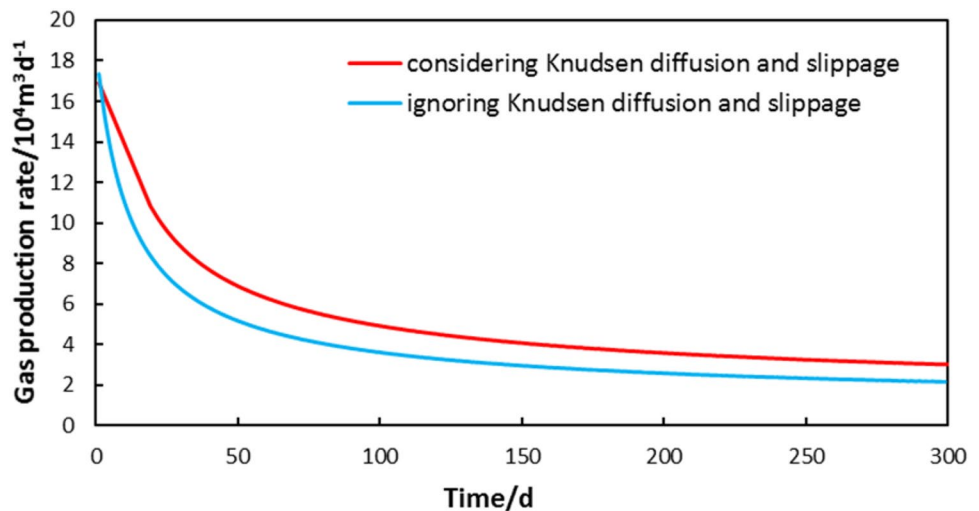

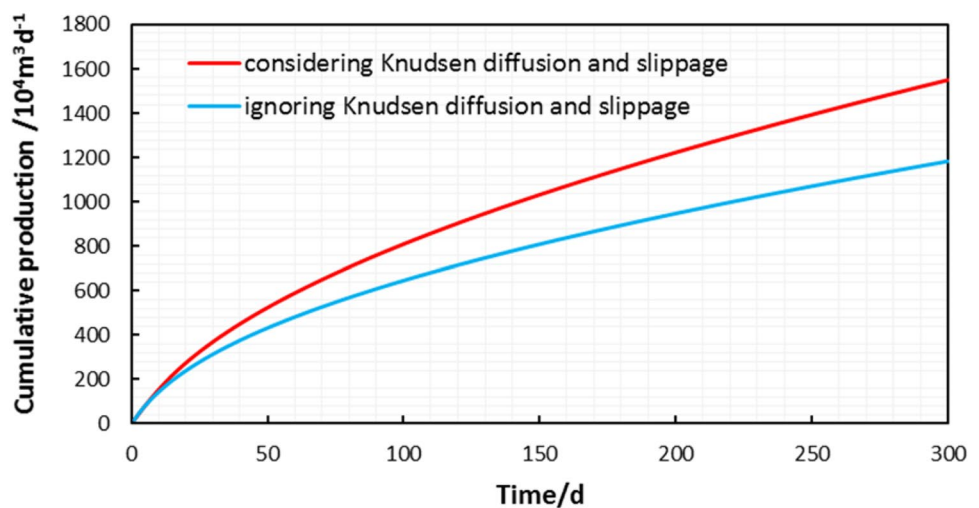**Fig. 9** Influence of Knudsen diffusion and slippage effect on cumulative production of well WH-1

Fig. 10 Influence of stress sensitivity on daily production of well WH-1
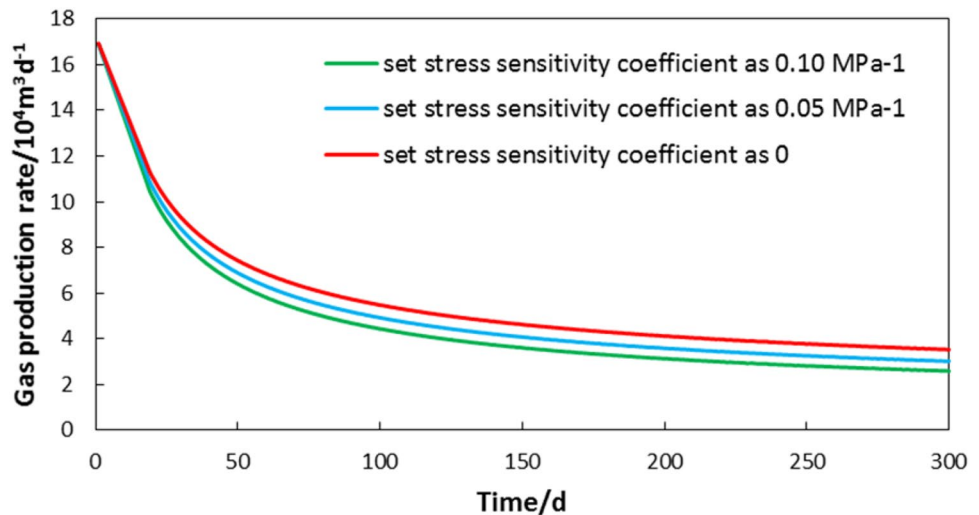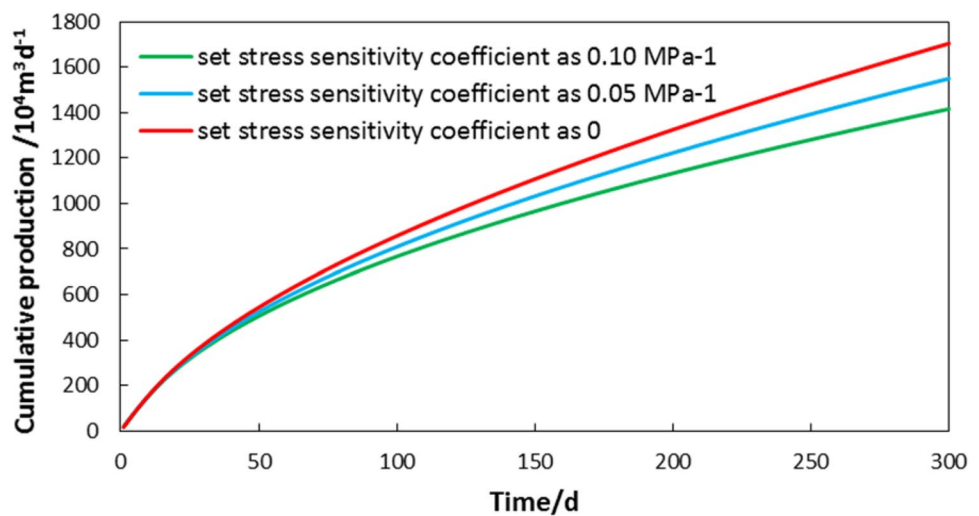

Fig. 11 Influence of stress sensitivity on cumulative production of well WH-1

terms cannot be substituted directly. The solutions of these problems are presented in Appendix 3 in detail.

Model verification

A real-case study of horizontal well WH-1 in Changning–Weiyuan shale gas reservoir has been used to validate the accuracy of this analytical model. Parameters of the gas reservoir are shown in Table 1 and the morphology of each fracture is shown in Table 2. The basic parameters are obtained by micro-seismic data in a productive scientific project, including fracture lengths, fracture orientations and so on. It demonstrates that fractures at arbitrary angles and asymmetric hydraulic fractures do exist, confirming the practical significance of this research.

The simulated daily gas production rate curve and actual production data curve are shown in Fig. 5. The average daily production values of actual data and simulation data in the

first 336 days are 5.020×10^4 m^3/day and 5.048×10^4 m^3/day, respectively. The difference between them is merely 0.558%, which verifies the accuracy of this novel model to predict production of horizontal well in fractured shale gas reservoir.

Results and discussion

Sensitivity analysis

In this part, production response was analyzed from the analytical solution of the novel mathematical model to help us better understand the sensitivity of some critical factors on productivity in practical shale gas fields, which in turn can serve as a guiding to optimize the fracturing design. The essential data are given in Tables 1 and 2.

Due to the multi-scale seepage mechanism of shale gas, certain factors may have a significant impact on production,

such as desorption, Knudsen diffusion, slippage flow, stress sensitivity and high-velocity non-Darcy flow. It is crucial to figure out whether these factors can impact production significantly and the extent of the impact. Based on the actual data in field, we conducted the single-variable method to study the sensitivity analysis under the effect of multi-scale seepage mechanism through the novel model.

Influence of desorption on production

Based on the basic data from WH-1, two different conditions were simulated to verify whether the impact of desorption

on production is significant or not. Consider desorption on the one hand and ignore desorption on the other hand when keeping the other input parameters unchanged, then the daily gas production curves and cumulative production curves are plotted in Figs. 6 and 7.

As shown in Figs. 6 and 7, the impact of desorption on gas production is large. The daily production in initial period seems high and decreases extremely; then the decline degree becomes gentle because early transient flow period transfers into late transient flow period. After that a relatively long and steady period called pseudo-steady production period is coming, which means that production extraordinarily

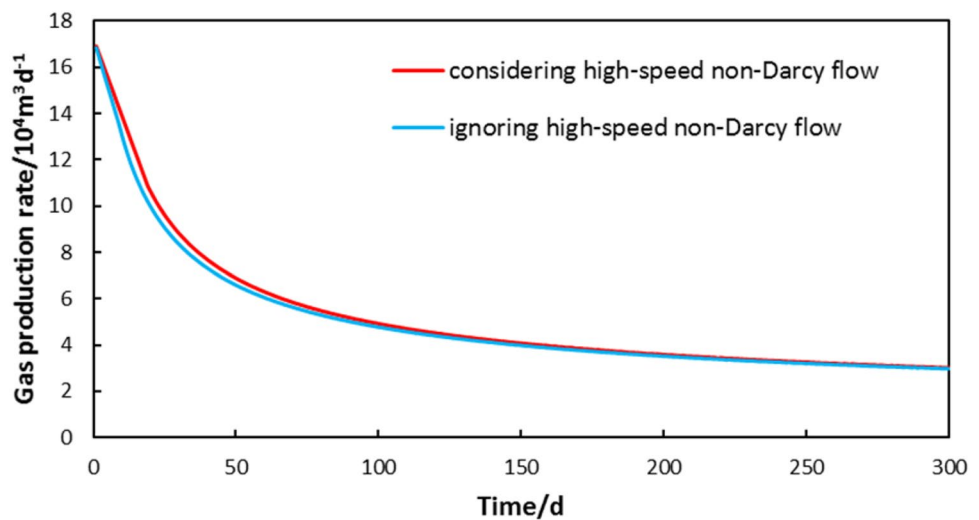**Fig. 12** Influence of high-speed non-Darcy flow on daily production of well WH-1

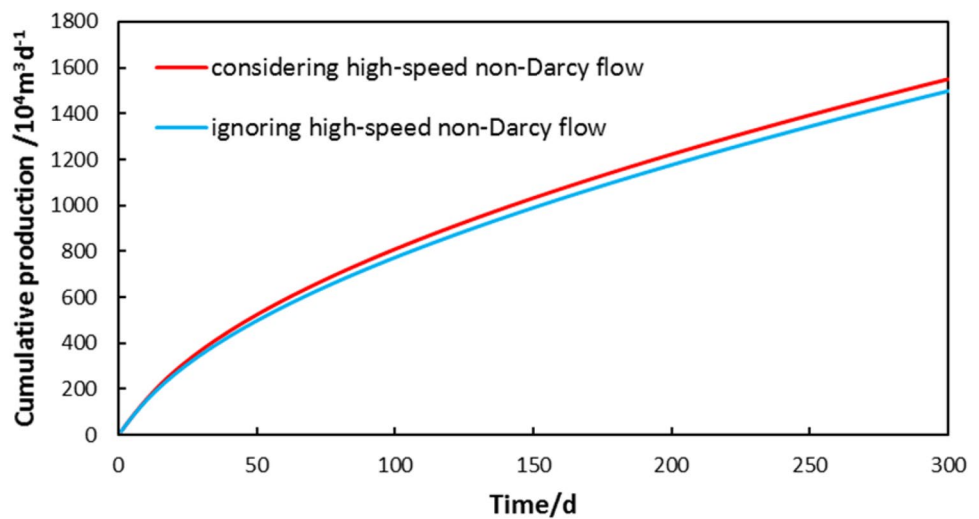**Fig. 13** Influence of high-speed non-Darcy flow on cumulative production of well WH-1

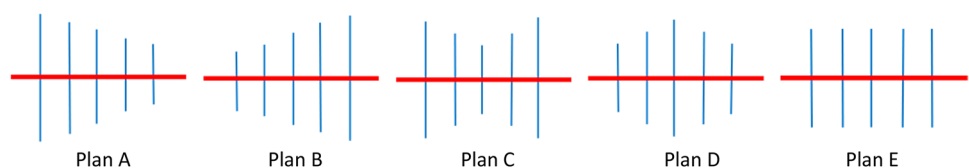**Fig. 14** Schematic of assemblies of different fracture length

Table 3 Different assemblies of fracture morphology

Section number	Plan A				Plan B				Plan C				Plan D				Plan E
	Len	I	L	R	Len	I	L	R	Len	I	L	R	Len	I	L	R	Len
1	120	115	115	115	110	130	120	110	120	130	110	120	110	100	120	110	115
2	120	115	115	115	110	130	120	110	120	130	110	120	110	100	110	120	115
3	120	115	115	115	110	130	120	110	120	120	110	120	110	110	120	110	115
4	120	115	115	115	110	120	120	110	120	120	110	120	110	110	110	120	115
5	120	115	115	115	110	120	120	110	120	110	110	120	110	120	120	110	115
6	115	115	115	115	115	120	120	110	110	110	110	120	120	120	110	120	115
7	115	115	115	115	115	120	120	110	110	100	110	120	120	130	120	110	115
8	115	115	115	115	115	110	120	110	110	110	110	120	120	120	110	120	115
9	115	115	115	115	115	110	120	110	110	110	110	120	120	120	120	110	115
10	110	115	115	115	120	110	120	110	120	120	110	120	110	110	110	120	115
11	110	115	115	115	120	100	120	110	120	120	110	120	110	110	120	110	115
12	110	115	115	115	120	100	120	110	120	130	110	120	110	100	110	120	115
13	110	115	115	115	120	100	120	110	120	130	110	120	110	100	120	110	115
14	110	–	115	115	120	–	120	110	120	–	110	120	110	–	110	120	115

Len half-length of hydraulic fracture, *I* interval between hydraulic fractures, *L/R* left/right side length of hydraulic fracture

approaches to constant. Different from conventional reservoirs, the production of initial period in shale gas reservoir is apparently higher due to desorption. There are usually two forms of shale gas in reservoir, namely free gas and adsorbed gas. In the early production time, the adsorbed gas will be desorbed from the surface of organic matter and flows into fracture network with free gas together when reservoir pressure starts dropping off. In later production time, the impact of desorption will decrease. However, this particular characteristic of shale makes lots of contribution to the production, which cannot be ignored in production prediction.

Influence of Knudsen diffusion and slippage effect on production

To analyze the impact of Knudsen diffusion and slippage effect on production, the production data of WH-1 were adopted to implement the simulation and figure out how this factor impacts the production. Consider or ignore Knudsen diffusion and slippage effect when still keeping the other input parameters invariant. Then we can obtain the daily production and cumulative production curves under the two different conditions.

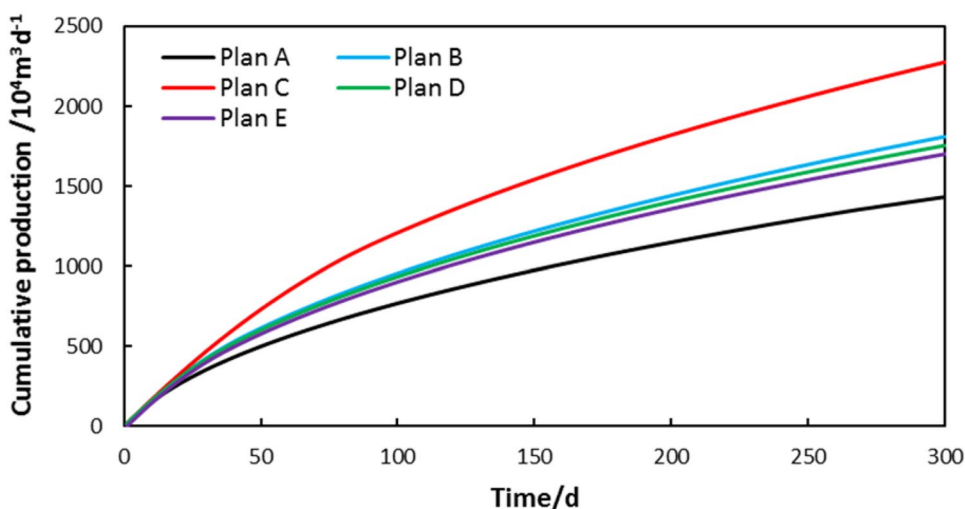**Fig. 15** The cumulative production impacted by different fracture length assemblies

Fig. 16 Schematic of assemblies of different intervals between fractures
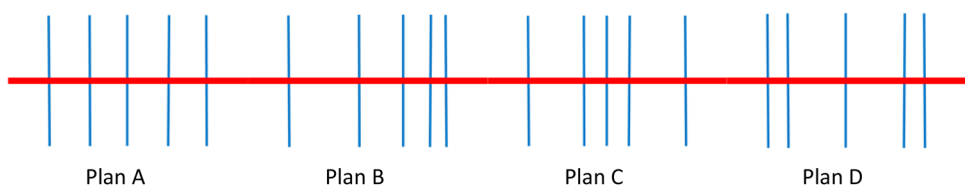

Fig. 17 The cumulative production impacted by different intervals between fractures
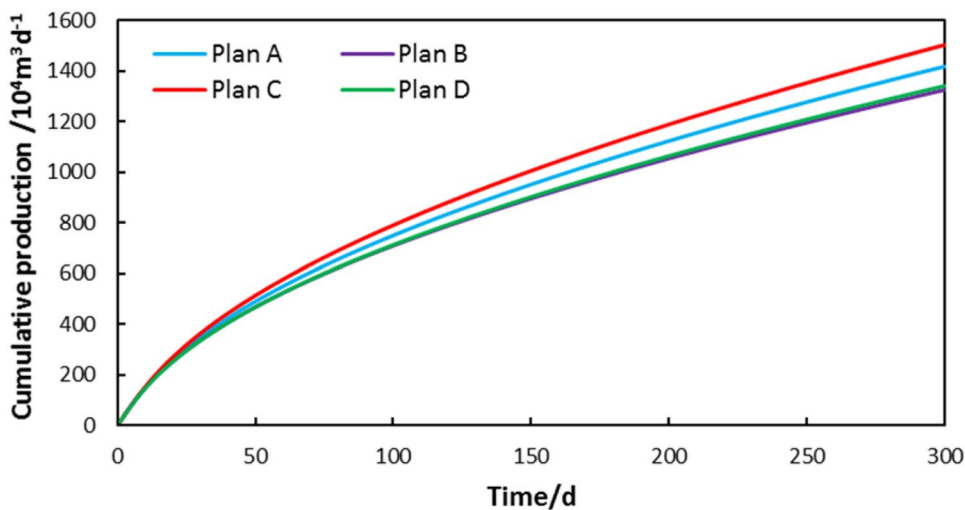
Fig. 18 Schematic of assemblies of different fracture symmetry

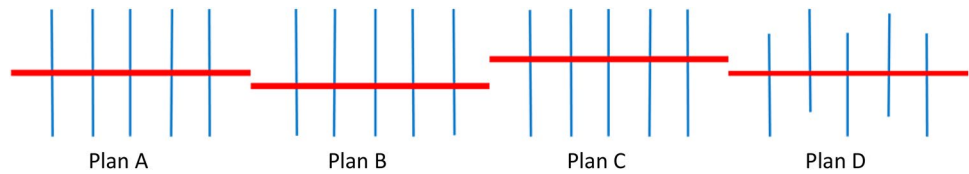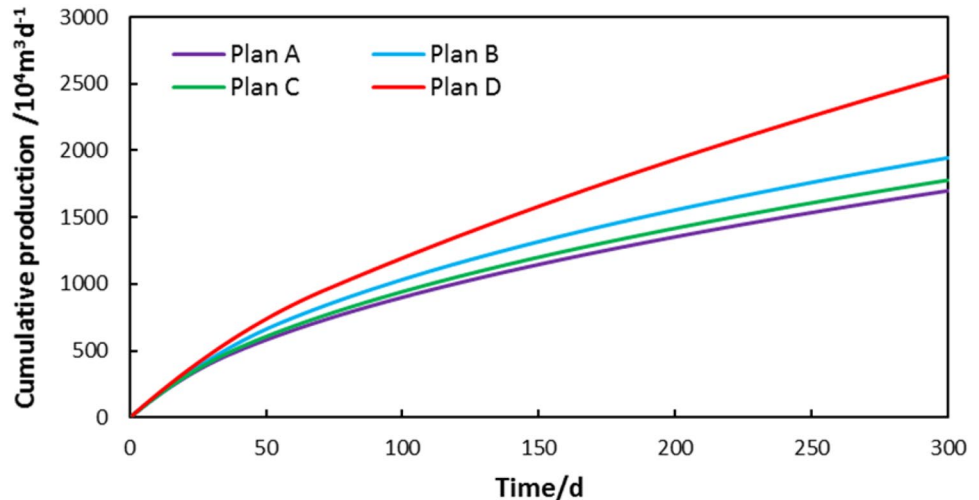Plan A   Plan B   Plan C   Plan D

Fig. 19 Cumulative production impacted by different fracture symmetry

As shown in Figs. 8 and 9, when Knudsen diffusion and slippage effect are taken into account, the gas production will increase in the whole process. What can account for the result is that the apparent permeability calculated by simulation is higher than the Darcy permeability gauged in static. When the pore diameter is similar to the free path of gas molecules, the chance that gas molecules collide with the surface of the pore will increase, and Knudsen diffusion plays a vital role in this process. That is why the apparent permeability we computed is higher than Darcy's so that productivity can ascend accordingly. It can be verified that Knudsen diffusion and slippage effect do have an influence on production of shale gas.

Influence of stress sensitivity on production

Set the coefficient of stress sensitivity as 0.1 MPa^{-1}, 0.05 MPa^{-1} and 0, and keep other input parameters unchanged. The daily production and cumulative production curves are also plotted in Figs. 10 and 11.

Figures 10 and 11 reveal that the influence of stress sensitivity can weaken the gas production. The reason exists in the specific tectonics of shale gas reservoir. There are generally enormous natural fractures and induced fractures caused by hydraulic fracturing in shale gas reservoirs. When formation pressure decreases, these micro-fractures may close, which will cause some reduction in production. Because of this phenomenon, the production will descend

mildly, namely the stress sensitivity just impacts production to a certain extent.

Influence of high-speed non-Darcy flow on production

To justify the impact of high-speed non-Darcy flow on production, we used the basic data of WH-1 as well to conduct the simulation. Similarly, by changing the existence of high-speed non-Darcy flow during the numerical simulation and keeping other input parameters unchanged, the daily production and cumulative production curves can be obtained, as shown in Figs. 12 and 13.

As shown in Figs. 12 and 13, we can see that high-speed non-Darcy flow has a slight effect on production. With the increase of production in early time, due to the extraction of free gas, the pressure of shale gas reservoir drops off sharply so that non-Darcy flow within the fractures gets enhanced. And production goes up as the response to this process. However, the daily production and cumulative production are slightly sensitive according to this factor, namely the influence of high-speed non-Darcy flow does not look so predominate on production even that we can ignore its impact or keep it as a constant when computational accuracy is not required to be so high.

Optimization of fracture morphology

In this section, we analyzed the influence of fracture morphology including fracture lengths, intervals and symmetry

distribution on gas production to optimize itself in turn. The cumulative production curves are plotted by setting different parameters. The basic parameters are shown in Tables 1 and 2.

Optimization of hydraulic fracture length

It is accessibly understood that when hydraulic fracturing is in process, short fractures are easy to create while long fractures are more helpful to enlarge SRV. However, the best assembly design of fracture length requests further study. Set five groups of different fracture length assembly: Plans A, B, C, D, E are ladder, anti-ladder, U-model, anti-U-model and symmetrical distribution, respectively, shown in Fig. 14 and Table 3. The simulation result is presented in Fig. 15.

Figure 15 shows that the cumulative production of Plan C is the highest among the five plans. It can provide a guide for engineers to optimize the fracture length more reasonably, which means that the design of longer outer fracture and shorter inner fracture in multistage fractured horizontal well deserves more attention from the designers of hydraulic fracturing treatment.

Optimization of hydraulic fracture interval

Set four groups of different assembly of fracture interval under the condition that the sum of all intervals in every plan is almost equal to each other. The conception of Plans A, B, C and D is visually shown in Fig. 16 and specific parameters are presented in Table 3, and the results are shown in Fig. 17.

As we can see from Fig. 17, the cumulative production of Plan C is higher than the other three plans. To obtain a larger gas production, the inner fracture intervals and the outer fracture intervals should be kept smaller and greater, respectively, as possible as we can under the reasonable conditions.

Optimization of hydraulic fracture symmetry

Four different plans are designed to analyze the impact of fracture symmetry on the cumulative production of multistage fractured horizontal well: symmetrical distributed fractures, asymmetrical distributed fractures and interlaced distributed fractures along the fractured horizontal wellbore (see Fig. 18; Table 3). The simulation results are shown in Fig. 19.

Figure 19 shows that the cumulative production of Plan D is the highest among the four plans, which means that interlaced fracture morphology has an advantage over the other designs. Theoretically, we should try our best to make hydraulic fractures interlaced along two sides of the horizontal wellbore to obtain more shale gas production.

It is necessary to notice that the assumptions aiming at easier analytical solution for the analytical model are the limitations of this method inevitably, which means these hypotheses are absolutely never existing and valid in practical conditions.

Conclusions

On the basis of corrected Warren and Root model, we have established a mathematical analytical model of multiple-staged fractured horizontal well in shale gas reservoir by physical description and mathematical expression, where the multi-scale seepage mechanism and the complicated morphology of hydraulic fractures were considered. Then reservoir was simplified into a radial composite Warren and Root model characterized by two different permeability of micro-fracture system, and the fractures have sealed outer boundary and limited conductivity in this model. We solved the model through modern well test method and mathematical physical method analytically. And in a certain extent, the results can play a guiding role in fracturing effect evaluation, fracturing operation design and proposal of post-fracturing production plan. After sequential researches, some conclusions are obtained.

1. 1. A novel model of shale gas production forecast in multiple fractured horizontal well has been established in this paper, where desorption, Knudsen diffusion and slippage flow, stress sensitivity of micro-fractures, and high-velocity non-Darcy flow within the main hydraulic fractures were taken into account based on the corrected Warren and Root model.
2. We applied well test analysis method to solve the mathematical model, and with the help of corrected Bessel function, the solution in Laplace space was obtained; then we acquired the analytical solution of the model with the assistance of numerical inversion.
3. The simulation program was compiled under the conception of Gauss elimination by visual basic program software, then adaptability and accuracy of the novel model is validated with the help of a real-case well WH-1 from Changning–Weiyuan shale gas reservoir.
4. By adopting the analytical method, the influence of desorption, Knudsen diffusion and slippage flow, stress sensitivity and high-velocity non-Darcy flow within the hydraulic fractures on production have been analyzed. The fracture morphology have been optimized through the simulation results, which can play a guiding role in fracturing design.
5. In terms of the optimization of fracture morphology, cumulative production of multistage fractured horizontal well tends to be higher under three following conditions: longer outer fractures and shorter inner fractures; greater outer fractures intervals and smaller inner frac-

tures intervals; interlaced fractures along the two sides of wellbore.

The innovation point of this mathematical model lies in its capability to calculate the post-fracturing production of more actual situation, such as fractures at arbitrary angles and asymmetric hydraulic fractures. The good accordance between calculation result and practical data verifies the accuracy and the applicability of this model. This paper is anticipated to play a guiding role in establishing the production forecast model of shale gas, and at some extent provides a reference for fracturing operation design and fractured production prediction in gas reservoirs, which are similar to shale gas reservoir such as tight gas reservoir and so on.

Appendix 1: Mathematical model

Shale gas flow in the micro-fractures is considered satisfying the Darcy law, whose motion equation is presented as follows (Li 2008):

$$\vec{v}_f = -3.6 \frac{K_f}{\bar{\mu}} \nabla p_f. \tag{19}$$

In terms of matrix and micro-fracture system, state equations are as follows, respectively:

$$\rho_m = \frac{M p_m}{\bar{Z} R T}, \tag{20}$$

$$\rho_f = \frac{M p_f}{\bar{Z} R T}. \tag{21}$$

If reservoir pressure is higher than critical desorption pressure, assuming that gas channeling process is steady when gas flows from matrix into micro-fracture system, channeling equation can be expressed when the apparent permeability K_{app} is considered (Cheng 2011):

$$q_{ex} = \frac{3.6 \sigma K_{app} \rho_g}{\bar{\mu}} (p_m - p_f), \tag{22}$$

$$\sigma = 4 \left(\frac{1}{L_x^2} + \frac{1}{L_y^2} + \frac{1}{L_z^2} \right), \tag{23}$$

where L_x, L_y and L_z are the characteristic lengths of cutting matrix in the directions of x, y, z, respectively.

As for continuity equations of micro-fractures and matrix system, they can be expressed as, respectively,

$$\frac{\partial (\phi_f \rho_f)}{\partial t} + \nabla \cdot \left(\rho_f \vec{v}_f \right) - q_{ex} = 0, \tag{24}$$

$$\frac{\partial (\phi_m \rho_m)}{\partial t} + q_{ex} = 0, \tag{25}$$

where ϕ_f and ϕ_m are porosities of micro-fracture and matrix.

It is inappropriate to use square pressure for calculation because shale gas cannot be thought as ideal gas. To linearize the percolation differential equation, we introduce pseudo-pressure into the model.

$$\frac{3.6 K_f}{\bar{\mu}} \left[\frac{1}{r} \frac{\partial}{\partial r} \left(r \frac{\partial \psi_f}{\partial r} \right) \right] + \frac{3.6 \sigma K_{app}}{\bar{\mu}} (\psi_m - \psi_f) = \phi_f C_{ft} \frac{\partial \psi_f}{\partial t}, \tag{26}$$

$$-\frac{3.6 \sigma K_{app}}{\bar{\mu}} (\psi_m - \psi_f) = \phi_m C_{mt} \frac{\partial \psi_f}{\partial t}, \tag{27}$$

where

$$\psi_f = 2 \int_0^{p_f} \frac{p}{\mu Z} dp,$$

$$\psi_m = 2 \int_0^{p_m} \frac{p}{\mu Z} dp,$$

$$C_{ft} = \frac{1}{p_f} - \frac{1}{\bar{Z}} \frac{\partial \bar{Z}}{\partial p_f},$$

$$C_{mt} = \frac{1}{p_m} - \frac{1}{\bar{Z}} \frac{\partial \bar{Z}}{\partial p_m}.$$

We find that desorption term has been offset during the calculation due to the limitation of the novel model, thus we superpose it after the model is deduced and add the amount of desorption gas, then the final results can be obtained.

Appendix 2: Model solution

Equation (7) is a constant problem, whose solution can be obtained easily as

$$\begin{cases} f_2(r) = \dfrac{1.274 \times 10^{-2} q_{sc} T}{K_f h (r_e^2 - r_w^2)} \left(r_e^2 \ln r - \dfrac{r^2}{2} \right) \\ \theta = \dfrac{9.173 \times 10^{-2} q_{sc} T}{\bar{\mu} h (\phi_m C_{mt} + \phi_f C_{ft})(r_e^2 - r_w^2)} \end{cases}, \tag{28}$$

Equation (8) is an unsteady problem, introducing the following:

$$\begin{cases} u_1 = e^{-vt}\Phi_1(r) \\ u_2 = e^{-vt}\Phi_2(r) \end{cases}.$$ (29)

Substituting it into Eq. (8), we obtain

$$\begin{cases} -v\Phi_1 = \xi(\Phi_2 - \Phi_1) \\ \dfrac{1}{r}\dfrac{\partial}{\partial r}\left(r\dfrac{\partial \Phi_2}{\partial r}\right) + \dfrac{\eta}{\xi}v\Phi_1 = -v\Phi_2 \\ \dfrac{\partial \Phi_2}{\partial r}\Big|_{r=r_e} = 0 \\ \dfrac{\partial \Phi_2}{\partial r}\Big|_{r=r_w} = 0 \end{cases},$$ (30)

in which ξ, η, λ, and X_2 have been explained and expressed in the preceding text; thus, an eigenvalue problem can be got

$$\begin{cases} \dfrac{d^2\Phi_2}{dr^2} + \dfrac{1}{r}\dfrac{d\Phi_2}{dr} + \dfrac{\lambda}{X_2}\Phi_2 = 0 \\ \dfrac{d\Phi_2}{dr}\Big|_{r_e} = \dfrac{d\Phi_2}{dr}\Big|_{r_w} = 0 \end{cases}.$$ (31)

On the one hand, as for $\Phi_2(r)$, consider $\Phi_2(r) = AJ_n\left(\sqrt{\frac{\lambda}{X_2}}r\right) + BY_n\left(\sqrt{\frac{\lambda}{X_2}}r\right)$, and we can obtain the equations as follows according to the boundary conditions:

$$\begin{cases} AJ_n\left(\sqrt{\dfrac{\lambda}{X_2}}r_e\right) + BY_n\left(\sqrt{\dfrac{\lambda}{X_2}}r_e\right) = 0 \\ AJ_n\left(\sqrt{\dfrac{\lambda}{X_2}}r_w\right) + BY_n\left(\sqrt{\dfrac{\lambda}{X_2}}r_w\right) = 0 \end{cases}.$$ (32)

Considering $\Phi_{1,0}(r, r_w, \lambda_j) = J_1\left(\sqrt{\frac{\lambda_j}{X_2}}r_w\right)Y_0\left(\sqrt{\frac{\lambda_j}{X_2}}r_e\right)$
$-Y_1\left(\sqrt{\frac{\lambda_j}{X_2}}r_w\right)J_0\left(\sqrt{\frac{\lambda_j}{X_2}}r_e\right)$, we can get

$$\Phi_2(r, r_w, 0) = \dfrac{1}{\left[\pi\left(r_e^2 - r_w^2\right)\right]^{\frac{1}{2}}}.$$ (33)

On the other hand, as for v, there is the equation:

$$v^2 - (\xi + \lambda + \eta)v + \xi\lambda = 0.$$ (34)

Solving the equation, we can obtain four roots of v:

$$\begin{cases} r_1 = v_{-j} = \dfrac{1}{2}\left[\xi + \eta + \lambda_j + \sqrt{(\xi + \eta + \lambda_j)^2 - 4\xi + \eta + \lambda_j}\right], & \lambda_j \neq 0, \, j = 1, 2, 3, \ldots \\ r_2 = v_{+j} = \dfrac{1}{2}\left[\xi + \eta + \lambda_j - \sqrt{(\xi + \eta + \lambda_j)^2 - 4\xi + \eta + \lambda_j}\right], & \lambda_j \neq 0, \, j = 1, 2, 3, \ldots \\ r_3 = v_{-j} = 0, \lambda_j = 0 \\ r_4 = v_{+j} = \xi + \eta, \lambda_j = 0 \end{cases}.$$ (35)

Considering $u_2 = \left[A_0 e^{-r_3 t} + B_0 e^{-r_4 t}\right]\Phi_2(r, r_w, 0) + \sum_{j=1}^{\infty}\left[A_1 e^{-r_1 t} + B_1 e^{-r_2 t}\right]\Phi_2(r, r_w, \lambda_j)$, combining the initial conditions this problem can be solved as follows:

$$\begin{aligned} u_2 = \psi_i &- \frac{1.274 \times 10^{-2} q_{sc} T r_e^2}{K_f h(r_e^2 - r_w^2)}\left[r_e^2\left(\ln r_e - \frac{1}{2}\right) - r_w^2\left(\ln r_w - \frac{1}{2}\right) - \frac{1}{4r_e^2}(r_e^4 - r_w^4)\right] \\ &- \frac{9.173 \times 10^{-2} q_{sc} T \eta}{\bar{\mu} h(\phi_m C_{mt} + \phi_f C_{ft})(r_e^2 - r_w^2)\xi(\xi + \eta)}\left[1 - e^{-(\xi + \eta)t}\right] + \frac{q_{sc} T}{2\bar{\mu} h \phi_f C_{ft} r_w \sqrt{X_2}\xi} \\ &\times \sum_{j=1}^{\infty} \frac{J_1^2\left(\sqrt{\frac{\lambda_j}{X_2}}r_e\right)\left[v_{+j}(\xi - v_{-j})e^{-v_{-j}t} - v_{-j}(\xi - v_{+j})e^{-v_{+j}t}\right]\Phi_{1,0}(r, r_w, \lambda_j)}{\sqrt{\lambda_j}(v_{+j} - v_{-j})\left[J_1^2\left(\sqrt{\frac{\lambda_j}{X_2}}r_w\right) - J_1^2\left(\sqrt{\frac{\lambda_j}{X_2}}r_e\right)\right]}. \end{aligned}$$ (36)

Substituting the two equations into Eq. (9):

$$
\begin{aligned}
\psi_{\mathrm{f}} = {} & \psi_{\mathrm{i}} - \frac{1.274 \times 10^{-2} q_{\mathrm{sc}} T}{K_{\mathrm{f}} h (r_{\mathrm{e}}^2 - r_{\mathrm{w}}^2)} \left[\frac{r^2}{2} + r_{\mathrm{e}}^2 \left(\ln r_{\mathrm{e}} - \frac{1}{2} \right) - r_{\mathrm{e}}^2 \ln r - r_{\mathrm{w}}^2 \left(\ln r_{\mathrm{w}} - \frac{1}{2} \right) - \frac{1}{4 r_{\mathrm{e}}^2} (r_{\mathrm{e}}^4 - r_{\mathrm{w}}^4) \right] \\
& - \frac{9.173 \times 10^{-2} q_{\mathrm{sc}} T t}{\bar{\mu} h (\phi_{\mathrm{m}} C_{\mathrm{mt}} + \phi_{\mathrm{f}} C_{\mathrm{ft}}) (r_{\mathrm{e}}^2 - r_{\mathrm{w}}^2)} - \frac{9.173 \times 10^{-2} q_{\mathrm{sc}} T \eta \left[1 - e^{-(\xi + \eta) t} \right]}{\bar{\mu} h (\phi_{\mathrm{m}} C_{\mathrm{mt}} + \phi_{\mathrm{f}} C_{\mathrm{ft}}) (r_{\mathrm{e}}^2 - r_{\mathrm{w}}^2) \xi (\xi + \eta)} + \frac{q_{\mathrm{sc}} T}{2 \bar{\mu} h \phi_{\mathrm{f}} C_{\mathrm{ft}} r_{\mathrm{w}} \sqrt{X_2} \xi} \\
& \times \sum_{j=1}^{\infty} \frac{J_1^2 \left(\sqrt{\frac{\lambda_j}{X_2}} r_{\mathrm{e}} \right) \left[\nu_{+j} (\xi - \nu_{-j}) e^{-\nu_{-j} t} - \nu_{-j} (\xi - \nu_{+j}) e^{-\nu_{+j} t} \right]}{\sqrt{\lambda_j} (\nu_{+j} - \nu_{-j}) \left[J_1^2 \left(\sqrt{\frac{\lambda_j}{X_2}} r_{\mathrm{w}} \right) - J_1^2 \left(\sqrt{\frac{\lambda_j}{X_2}} r_{\mathrm{e}} \right) \right]} \, \Phi_{1,0} (r, r_{\mathrm{w}}, \lambda_j).
\end{aligned}
\tag{37}
$$

Appendix 3: Calculation of the pseudo-pressure

In this part, according to the conclusion of Tian et al. (2009), an empirical equation has been used to calculate the pseudo-pressure of imperfect gas, which is expressed as

$$
\psi_i = \int_0^{p_i} \frac{2p}{\mu Z} \mathrm{d}p = \int_0^{p_z} \frac{2p}{a_1 + a_2 p + a_3 p^2} \mathrm{d}p + \int_{p_z}^{p_i} \frac{2p}{b_1 + b_2 p} \mathrm{d}p,
\tag{38}
$$

where a_1, a_2, a_3, b_1, b_2 can be expressed as

$$
a_1 = \left(-1.4509 e - 4 T^2 + 0.3647 T + 105.3525 \right) / 10{,}000,
$$

$$
\begin{aligned}
a_2 = {} & \left(1.9862 e - 7 T^3 - 1.0590 e - 4 T^2 + 2.9997 e \right. \\
& \left. -2 T - 2.6249 \right) / 10{,}000,
\end{aligned}
$$

$$
\begin{aligned}
a_3 = {} & \left(3.9391 e - 8 T^3 - 1.7025 e - 4 T^2 + 3.028 e \right. \\
& \left. -3 T - 0.2708 \right) / 10{,}000,
\end{aligned}
$$

$$
b_1 = \left(-6.3629 e - 4 T^2 + 0.7805 T - 25.9972 \right) / 10{,}000,
$$

$$
\begin{aligned}
b_2 = {} & \left(-6.463 e - 7 T^3 + 3.0357 e - 4 T^2 - 6.2120 e \right. \\
& \left. -4 T + 9.4704 \right) / 10{,}000.
\end{aligned}
$$

In addition, p_z is the conversion pressure changing with reservoir pressure, which is calculated as follows in this paper:

$$
p_z = 0.1 T + 15.
\tag{39}
$$

References

Bustin A, Bustin RM, Cui X (2008) Importance of fabric on the production of gas shales. In: SPE unconventional reservoirs conference. Society of Petroleum Engineers. https://doi.org/10.2118/114167-MS

Chen ZX (1983) Exact solution to the problem of flow of slightly compressible fluids in a bounded confined "practure-pore" medium and its application to well testing. Applied Mathematics Mechanics 4(3):435–447

Cheng L (2011) Advanced seepage mechanics. Petroleum Industry Press, Beijing

Civan F, Rai CS, Sondergeld CH (2011) Shale-gas permeability and diffusivity inferred by improved formulation of relevant retention and transport mechanisms. Transp Porous Media 86(3):925–944

Duan Y, Wei M, Li J, Tang Y (2011) Shale gas seepage mechanism and fractured wells' production evaluation. J Chongqing Univ 34(4):63–66

Fan H, Zhang Q, Wang N, Wang X (2013) Productivity prediction of a finite-conductivity fracture horizontal well in low permeability gas reservoir. Well Test 22(3):1–4

Frantz JH, Williamson JR, Water K et al (2005) Evaluating Barnett shale production performance-using an integrated approach. In: SPE annual technical conference and exhibition. Society of Petroleum Engineers. https://doi.org/10.2118/96917-MS

Guo J, Zhang L, Wang H, Feng G (2012) Pressure transient analysis for multi-stage fractured horizontal wells in shale gas reservoirs. Transp Porous Media 93(3):635–653

Javadpour F (2009) Nanopores and apparent permeability of gas flow in mudrocks (shales and siltstone). J Can Pet Technol 48(8):16–21

Kucuk F, Sawyer WK (1980) Transient flow in naturally fractured reservoirs and its application to Devonian gas shales. In: SPE annual technical conference and exhibition. Society of Petroleum Engineers. https://doi.org/10.2118/9397-MS

Lang Z, Zhang L, Cheng L (1994) Investigation on productivity of fractured horizontal well. J Univ Pet China 18(2):43–46

Li X (2008) Seepage mechanics of underground oil and gas. Petroleum Industry Press, Peking

Liu P, Yang H (2008) The formula about productivity forecast at the condition of low velocity non-Darcy percolation. Well Test 17(6):19–21

Mukherjee H, Economides MJ (1991) A parametric comparison of horizontal and vertical well performance. SPE Form Eval 6(2):209–216

Ozkan E, Raghavan RS, Apaydin OG (2010) Modeling of fluid transfer from shale matrix to fracture network. In: SPE annual technical conference and exhibition. Society of Petroleum Engineers. https://doi.org/10.2118/134830-MS

Raghavan R, Joshi SD (1993) Productivity of multiple drainholes or fractured horizontal wells. SPE Form Eval 8(1):11–16

Rahman MM (2008) Productivity prediction for fractured wells in tight sand gas reservoirs accounting for non-Darcy effects. In: The Russian oil and gas technical conference and exhibition. Society of Petroleum Engineers. https://doi.org/10.2118/115611-MS

Spivey JP, Semmelbeck ME (1995) Forecasting long-term gas production of dewatered coal seams and fractured gas shales. Tree Physiol 30(1):32–44

Swami V, Settari A (2012) A pore scale gas flow model for shale gas reservoir. In: SPE Americas unconventional resources conference.

Society of Petroleum Engineers. https://doi.org/10.2118/155756-MS

Tian J, Li C, Huang S et al (2009) A new empirical formula of pseudo pressure calculation for real gas. Oil Drill Prod Technol 31(2):65–67

Wu X (2008) Mathematical physics equation and its application. Science Press, Peking

Wu YS, Moridis G, Bai B et al (2009) A multi-continuum model for gas production in tight fractured reservoirs. In: SPE hydraulic fracturing technology conference. Society of Petroleum Engineers. https://doi.org/10.2118/118944-MS

Xu Y, Qi T, Yang F, Li H, Zhou S (2006) A new production forecast model of post-frac horizontal well. J Pet 27(1):89–91

Zhang X, Du C, Deimbacher F et al (2009) Sensitivity studies of horizontal wells with hydraulic fractures in shale gas reservoirs. In: International petroleum technology conference. Society of Petroleum Engineers. https://doi.org/10.2523/IPTC-13338-MS

Zhang D, Zhang L, Zhao Y, Guo J (2015) A composite model to analyze the decline performance of a multiple fractured horizontal well in shale reservoirs. J Nat Gas Sci Eng 26:999–1010

Zhao J, Pu X, Li Y, He X (2016) A semi-analytical mathematical model for predicting well performance of a multistage hydraulically fractured horizontal well in naturally fractured tight sandstone gas reservoir. J Nat Gas Sci Eng 32:273–291